Journal of Materials Chemistry A

Accepted Manuscript

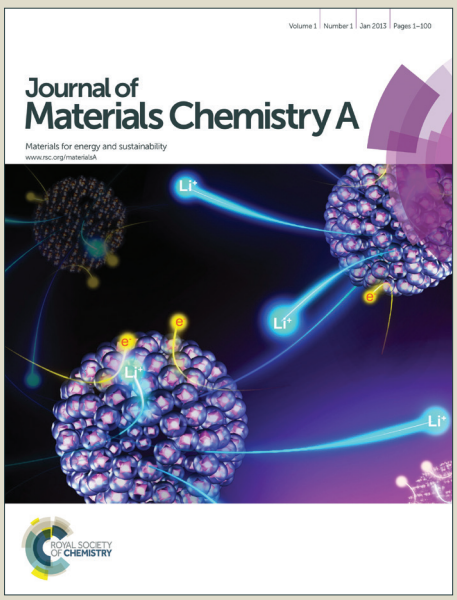

ROYAL SOCIETY OF CHEMISTRY

www.rsc.org/materialsA

Silicon/graphene based nanocomposite anode: massive production and stable high capacity for lithium ion batteries

Renzong Hu, Wei Sun, Yulong Chen, Meiqin Zeng, and Min Zhu*

School of Materials Science and Engineering, South China University of Technology
Key Laboratory of Advanced Energy Storage Materials of Guangdong Province, Guangzhou 510640, P.R. China

*Corresponding author.
Tel.:+86-20-87113924; fax: +86-20-87111317
E-mail: memzhu@scut.edu.cn

Abstract:

A Si/graphene nanocomposite, with nano-Si particles tightly wrapped and connected by graphene nanosheets, was prepared at large scale by using discharge-plasma-assisted milling (P-milling). The nanocomposite with 50wt% Si demonstrated high capacity, good cycleability, and excellent high-rate capability as a lithium storage anode, which delivered a discharge capacity of 866 $mAhg^{-1}$ and coulombic efficiency above 99.0% after 200 cycles under a current density of 0.4$mAcm^{-2}$. The capacity loss above 200 cycles was only ~0.07% per cycle among 0.02-2V. The practical relevance of this anode was further confirmed by a full coin-type cell with a $LiMn_2O_4$ cathode, which could cycle with stable capacities at practical working voltage between 3.2 and 4.2 V. Moreover, micro-Si mixed with WC and graphite was also treated by P-milling to form a "core-shell-shell" Si-WC/graphene nanocomposite with better cycleablity. These superior electrochemical properties were attributed to the highly enhanced structure stability and conductivity of the nanocomposite electrodes due to the complete coating of the micro/nano-Si particles by the graphene nanosheets. The present Si/graphene based nanocomposite may have good potential for large-scale applications because of the cost-effective and easy scalability of its synthesis by P-milling processes.

Graphic Abstract

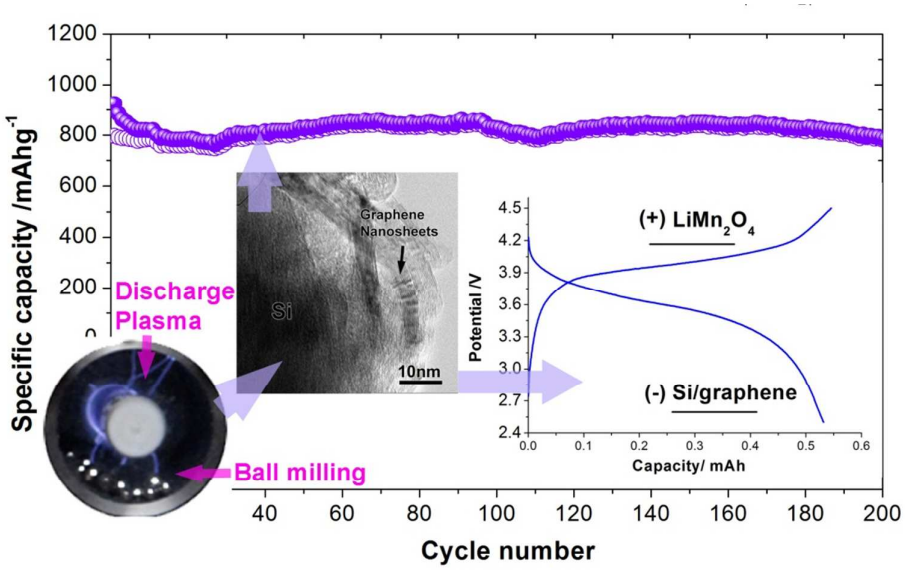

Plasma-assisted milled Si/graphene nanocomposite anode delivers high capacity and good cycleability in half and full cells using a $LiMn_2O_4$ cathode.

1. Introduction

In recent years, increasing energy density is a key point for optimizing the use of lithium ion batteries (LIBs) in an extended range of applications, especially electric /hybrid vehicles and smart grids. However, such a goal cannot be reached by using commercial graphite anodes, which have the obvious disadvantages of limited capacity (372 $mAhg^{-1}$) and safety issues. Thus, there was a strong demand in the last decade for the development of new anode materials of higher specific energy.[1–4] Among the possible candidates, silicon has attracted great interest because it has the highest theoretical capacity (4200mAh g^{-1} vs. $Li_{4.4}Si$), and is safer than graphite (the voltage plateaus of Li–Si alloying are higher than those of Li–C).[5–8]

However, the practical use of pure Si as an anode in LIBs is still hindered by two major challenges namely, the low electric conductivity and especially severe volume changes (>300%) during the Li insertion/extraction process, which lead to inferior rate capability and poor cycling performance. Many studies have been performed to overcome these problems by reducing the Si particle size,[8–10] producing three-dimensional porous structures,[11,12] creating silicon–metal alloys,[13,14] and dispersing nano-Si into a conductive inactive/active matrix,[5,15–20] and so forth. In these approaches, the Si/carbon composite anodes show their potential in improving the overall electrochemical performance of the anodes for LIBs by combining the advantages of different nanocarbon netwoks and Si. [5, 7, 12, 16–20, 21]

Owning to its unique physical and chemical properties including high electronic conductivity, excellent mechanical flexibility, superior chemical stability, and large theoretical specific surface area, graphene and graphene nanosheets have been used as a flexible carbonaceous coating to construct different dimensions of Si-based electrode materials by various strategies. [11, 22-24] In these materials, the graphene nanosheets were usually produced by mechanical peeling-off of graphite, chemical vapor deposition (CVD), and chemical or thermal reduction from graphite oxide. For example, Ma *et al.* synthesized a novel lily-like microparticles consisting of graphene nanosheet-wrapped Si nanoparticles anode based on a spray drying process and subsequent thermal treatment. [22] Guo *et al.* prepared highly wrinkled graphene nanosheets coated Si nanoparticles by combining freeze-drying and thermal reduction processes. [23] The as-obtained hybrids exhibited a remarkably improved cycling performance and rate performance in comparison with bare Si nanoparticles, which was attributed to the unique structure of the hybrids. However, for these Si-based anode materials, many difficulties still exist in the utilization of graphene /graphene

nanosheets by the mechanical peeling-off of graphite and CVD may be complex and expensive for mass production. Widely reported preparation routes for Si/graphene nanosheet composites based on graphite oxide require harsh conditions such as strong oxidizing and reducing reagents, high temperature, and precise times and reactant ratios, leading to a laborious and time-consuming preparation process.[23-26] And furthermore, although some properties of these complex designed Si-based anodes far exceed those of the conventional graphitic anode materials, the overall performance of these Si-graphene anode materials, especially cycle performance, output of materials, electrode loading, or capacity per unit area, are still far from practical applications.

In contrast to the rather complicated chemical synthesis (vapor deposit, sol–gel, pyrolysis, hydrothermal method, etc.), various ball milling processes for preparing Si-carbon nanocomposites have attracted more attentions. [8, 16, 27-30] The popularity of these methods and materials is due to their cost-effectiveness and applicability for large-scale manufacturing. Recently, Chen et al. prepared a core–shell-structured Si/B_4C composite with a coating of a few graphitic layers using a two-step ball milling method, and obtained long-term stability with a specific capacity of ~822 mAh g^{-1} and ~94% capacity retention over 100 cycles.[30] In this material, B_4C with high hardness serves as micro- or nanomiller that breaks down the micro-Si, and as conductive rigid skeleton that support the Si particles and thereby alleviates the volume expansion during charge/discharge.

In our previous study, we prepared Sn–C nanocomposites on a large scale by high-efficiency discharge-plasma-assisted milling (P-milling).[31,32] P-milling exerted a significant synergy effect, which is a combination of rapid heating by the plasma and milling impact stress on the Sn/graphite powders. Thus, the Sn particles were quickly refined and well dispersed in the nanosized graphite matrix. This led to the highly enhanced cyclic performance of the anode for LIBs. The functions of the discharge plasma on the refining of materials with various dielectric constants was carefully discussed in our papers.[33,34]

In this work, one-step synthesis of a Si/graphene nanocomposite was achieved by the P-milling method for the first time. Moreover, micro-Si mixed with wolfram carbide (WC) and graphite was also treated by P-milling for comparison, in which the rigid WC particles were expected to refine the micro-Si in milling, and also act as the cornerstones for the Si to withstand their pulverizations and aggregations. It was found that nano-Si as well as the submicro-sized WC particles could also act as millers that break down the graphite to form many graphene nanosheets, which in turn coated

and connected the Si nanoparticles and ensured their high structure stability and conductivity. The Si/graphene based nanocomposite anodes showed markedly improved Li storage performance, especially high capacity and superior cycling performance in half and full cells using $LiMn_2O_4$ as cathode.

2. Experimental

2.1 Preparation of Si/graphene nanocomposite

The raw materials used in this study were natural graphite powder (~30μm, 99.9% pure), WC powder (1~2μm, 99% pure), micro-sized Si powder (1~3μm, 99% pure), and 99.9% pure nano-Si with an average particle size of 100 nm. Their morphologies can be seen in **Figure S1 (Supporting Information)**. According to our previous investigation on P-milled Sn/graphite composite anodes,[31, 32] the powders (0.2kg) with nano-Si/C weight ratio of 50/50 were mixed and treated by P-milling for 10h to obtain the composite of Si/graphene nanosheets. Details of the P-milling method were carefully described in our previous publications.[33, 34] The ball mill was a vibration type and the milling cylinder vibrated with double amplitude of 7 mm and a frequency of 24 Hz. The weight ratio of stainless steel ball to powder was 40:1. In the milling process, the powder mixtures were sealed in a stainless steel vial under an argon atmosphere, which also served as an agent for the discharge plasma generation during milling. For comparison, the pure graphite sample was also treated by P-milling for 10 h, and the nano-Si/graphite powder mixtures were milled for 10h without plasma assistance (a process here after referred to as C-milling). The Si-WC/graphene nanocomposite (Si: WC: C, 20: 30: 50 wt %) was prepared by C-milling the mixture of micro-Si and WC powder for 15h and then by P-milling the Si-WC composite with graphite for 10h. These anodes were tested for references.

2.2 Material characterization

The structure and morphology of the samples were characterized by using a Philips X-ray diffractometer with Cu-K_α radiation, a Carl Zeiss Supra 40 field emission scanning electron microscope, a JEM-2100 transmission electron microscope (TEM) operating at 200 kV, and a laser Raman spectrometer (LabRam Aramis) at an excitation wavelength of 632.8 nm. In order to retain the original morphology of the products, the as-prepared sample powders were directly dispersed on Cu grids for TEM measurements.

2.3 Electrochemical measurements

The discharge–charge cycling performance of the samples was investigated using cell test systems (LAND-CT2001A, Arbin BT-2000) with CR2016 coin-type cells assembled in an argon-filled glove box. The working electrodes consisted of 80 wt% of the various active materials,

10 wt% conductivity agent (Super-P), and 10 wt% binder (polyvinyldifluoride). The mass loading was among 1.5-1.8 mg cm^{-2} for the electrodes. Lithium foil was used both as counter electrode and as reference electrode in the half cells. The electrolyte was $LiPF_6$ (1 mol L^{-1}) in a mixture of ethylene carbonate (EC)/diethyl carbonate (DEC)/ethyl methyl carbonate (EMC) with volume ratio EC/DEC/EMC=1:1:1. The cells were tested at various current densities among different voltage ranges at room temperature. Cyclic voltammetry (CV) over the potential range of 0.0–2.0 V at a scan rate of 0.3 mVs^{-1}, as well as impedance spectroscopy at 10mV amplitude signal in the 1MHz to 0.01 Hz frequency range, was performed by using a Gamry Interface 1000 Electrochemical System. A coin-type full cell with the Si/graphene nanocomposite anode and a $LiMn_2O_4$ cathode was assembled and cycled between 2.5 and 4.5V at a current of 0.4mA.

3. Results and Discussion

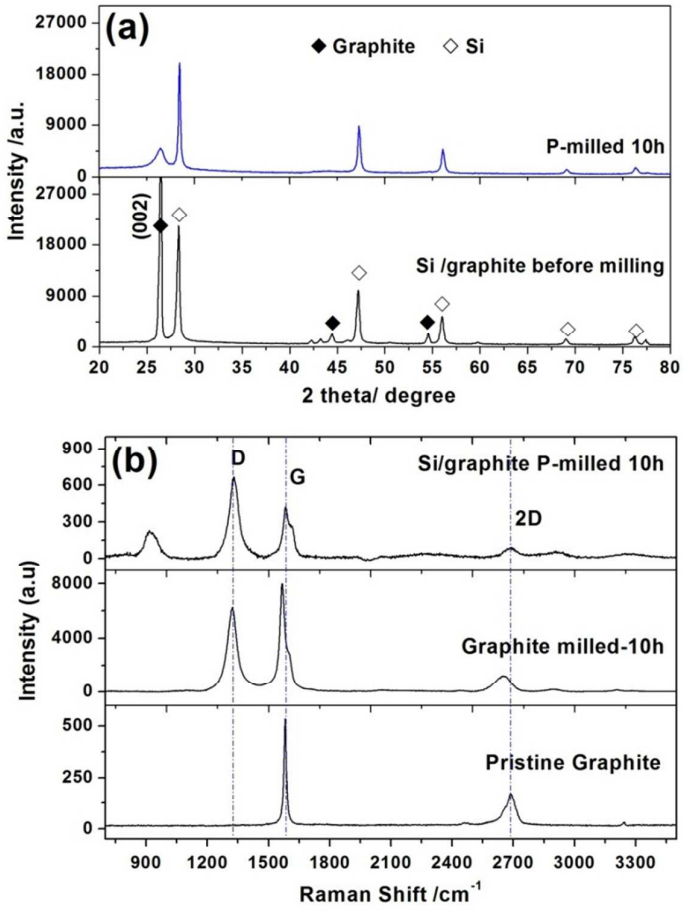

Figure 1. (a) XRD patterns of the Si/graphite composite before and after 10h P-milling; and (b) Raman spectra of the P-milled Si/graphite composite, pristine graphite, and graphite after P-milling for 10h.

Figure 1a shows the X-ray diffraction pattern of the Si/graphite powder before and after

milling for 10 h. Diffraction peaks of carbon and Si of the composite milled for 10h can be clearly observed, whereas no peak corresponding to SiC can be seen. The (002) peak of graphite obviously broadened as the milling time increased (see **Figure S2**, **Supporting Information**), as indicated by the increase in full width at half-maximum of the (002) peak from 0.162 before milling to 0.713 after 10 h milling. This broadening suggests that the graphite particles had been dramatically reduced in size along the *c* direction via formation of graphene nanosheets during milling. By contrast, the characteristic peaks of the Si phase apparently did not change, suggesting that the size changes of Si particles are not apparent as compared with those of graphite. This is quite different from the recent reported C-milled pure Si with partially amorphization, which had been found that the amount of amorphous Si increases with milling time (from 10 to 30h), as the microsized crystal Si particles were treated by high energy mechanical milling (900 rpm). [35] However, during P-milling of nano-Si/graphite powders, there was not obvious amorphization of Si. This should be attributed to the rapid heating by the plasma and the initial nanocrystalline nature (~100nm) of nano-Si particles, as well as that the lubrication of graphite much reduces the pressure performed on the Si. This leaded to that the pressure was below the driving force for the milled-induced amorphization of materials.[36]

Figure 1b shows the Raman spectra of P-milled Si/graphite composite, pristine graphite, and P-milled graphite. The spectrum of pristine graphite shows no detectable D band, but G and 2D bands are apparent at 1582 and 2686 cm^{-1}, respectively, [37] and the ratio of D- to G-band intensities (I_D/I_G) was zero. In contrast, Si/graphite composite and P-milled graphite produced strong D bands at around 1340 cm^{-1}, and their I_D/I_G ratios were 1.84 and 0.766, respectively. These bands indicate that significant size reduction of graphite by mechanical cracking and edge distortion occurred because of the significant synergy between the rapid plasma heating and milling impact stress. Notably, the I_D/I_G ratio of the P-milled Si/graphite composite was much larger than that of the P-milled pure graphite, indicating that the graphite in the composite underwent further crushing and refining than did pure graphite although both were treated P-milled for the same duration (10h). This result may be due to role of nano-Si particles as nanomillers, which assisted the steel balls and the discharge plasma in refining the graphite. Thus, more graphene formed in the Si/graphite composite.

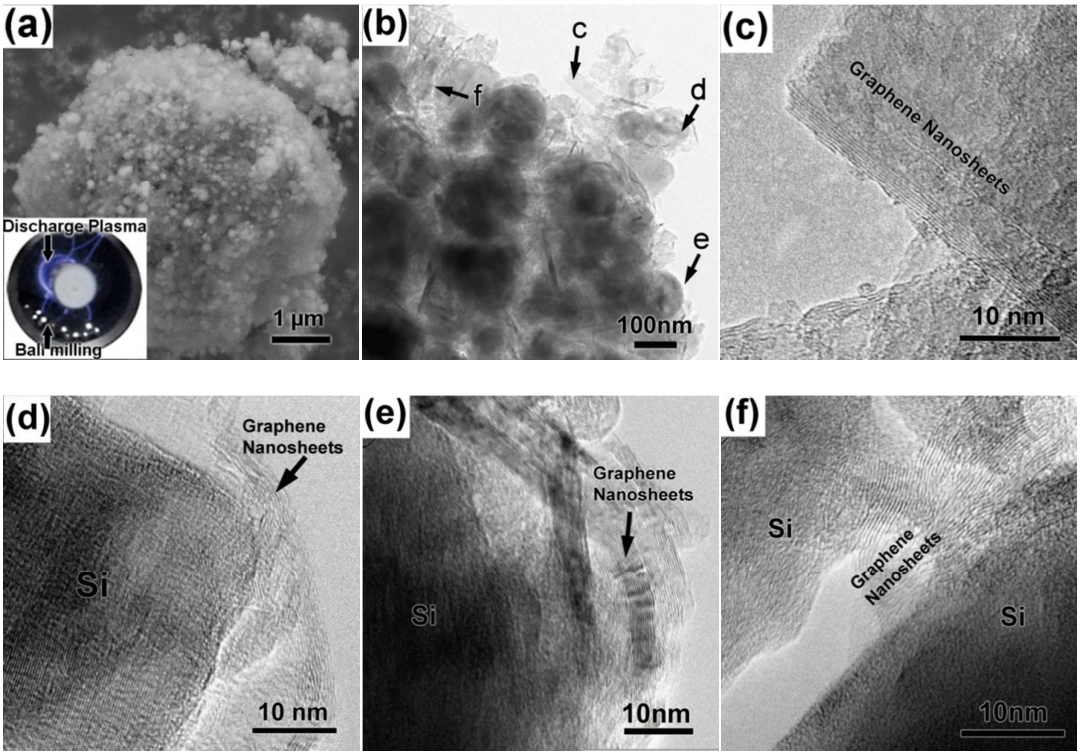

Figure 2. (a) SEM image and (b) TEM image of the P-milled Si/graphite composite; and (c–f) magnified images of zones *c–f* indicated by arrows in (b), respectively, showing the nano-Si particles coated and connected by graphene nanosheets.

Figure 2a shows the scanning electron microscopy (SEM) image of the P-milled Si/graphite composite, while the insert in left bottom is an image of the dielectric discharge plasma assisted milling, showing the plasma and the balls acted on the composite during milling. In contrast to the initial morphology of the composite (see **Figure S1(a)**), that of the large graphite sheets showed fragments. Microsized spherical granules formed and the nano-Si particles were dispersed uniformly in the graphite matrix (**Figure S3 (a)**, **Supporting Information**) after P-milling for 10h, while the high magnification SEM image (**Figure S3 (b)**) clear shows the complete coating of nano-Si particles by the thinned graphite flakes. The TEM image in **Figure 2b** further shows that the spherical nano-Si particles were dispersed well in the graphite matrix, whereas the graphite matrix was composed of many graphene nanosheets. **Figure 2c–f** respectively display magnified images of zones *c–f* indicated by arrows in Figure 2b. A graphene nanosheet presumed to have peeled off from the microsized graphite sheets during P-milling is shown in **Figure 2c**. **Figure 2d** and **2e** clearly shows that each nano-Si particle had been coated by 20 graphene nanosheets of less

than 10 nm thickness. The distortion and close attachment of the graphene nanosheets to the surface of the nano-Si particles, may be attributed to the effects of rapid heating by the plasma and impact stress by the steel balls during milling. As shown in **Figure 2f**, some graphene nanosheets also formed bridges between the nano-Si particles. On the basis of the above microstructure investigations, we can conclude that the Si/graphene nanocomposite anode with graphene nanosheets uniformly coated on nano-Si particles were successfully prepared in one step by P-milling. These preparation approaches are much more cost-effective and easy to scale up (to kg scale) compared with processes involving chemical reactions.[19,25, 26,38–41] Therefore, it has a good potential to be used for large-scale applications. Since the graphene nanosheet matrix is flexible and highly conductive, a composite electrode based on such structure can accommodate the large volumetric changes of the Si particles during discharge/charge cycling.

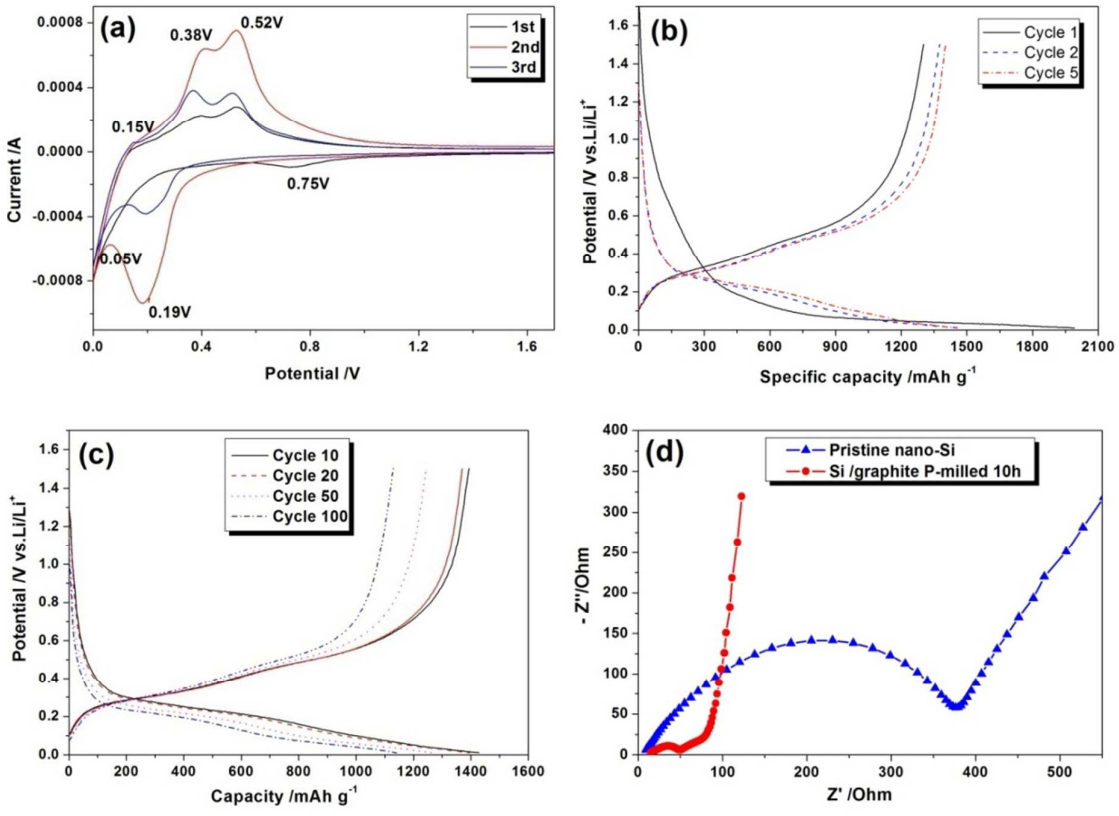

Figure 3. Electrochemical performance of the P-milled nano-Si/graphite composite anode: (a) CV curves obtained at a scanning rate of 0.3mVs^{-1}; (b and c) discharge–charge profiles at 0.4mAcm^{-2}current density between 0.01and 1.5V; and (d) impedance responses of the cells after the first cycle and of the pristine nano-Si electrode.

The electrochemical performance of the Si/graphene nanocomposite used as anode was first

investigated by CV. Typical voltammograms of the half cell in the first scan (**Figure 3a**) show two cathodic peaks (at ~0.05 and 0.75V) and three anodic peaks (at ~0.15, 0.38, and 0.52 V). In the subsequent scans, another cathodic peak at ~0.19V appeared. The 0.75V peak might be induced by electrolyte decomposition and formation of a solid electrolyte interface (SEI) film on the edge distortions and topological defects of the graphene nanosheets.[42] Cathodic and anodic peaks ~0.05 and ~0.15 V, respectively are due to reaction of Li with graphene in the composites. The cathodic peak at ~0.19 V and the anodic peaks at 0.38 and 0.52 V are characteristic peaks for the reaction of Li with Si.[6,8] The obvious increase in intensity of the peaks could be attributed to the considerably large amount of remaining crystalline Si in the inner particles that gradually reacted with Li during repeated discharge and charge.

Figure 3b shows the initial five charge/discharge profiles of the Si/graphene nanocomposite anode at 0.4mAcm^{-2} between 0.01 and 1.5V. Notably, a very high initial discharge (lithiation) /charge (delithiation) capacity of about 1992 and 1302mAhg^{-1} corresponding to an initial coulombic efficiency of 65.4% was obtained. During the first discharge process, the voltage steeply decreased to about 0.20–0.10V, and then slowly decreased to 0.01V. Discharging/charging profiles from subsequent cycles show smooth sloping curves, with average lithiation and delithiation potentials at 0.20 and 0.40V, respectively. These phenomena are consistent with the previously reported electrochemical behavior of anodes constructed from milled Si–carbon nanocomposite.[20,21,28,35] **Figure 3c** shows the discharge–charge profiles of a few representative prolonging cycles (cycles 10, 20, 50, and 100) for the composite anode. Retention of the voltage trend of this electrode in all cycles confirms the good reversibility of the reactions at the composite electrode. This reversibility is attributed to the enhanced structural stability and conductivity of the electrodes resulting from the highly conductive and fixable graphene nanosheets. The effect of graphene nanosheets on the conductivity of the composite electrode was demonstrated by the dramatic change in impedance of the Si/graphene nanocomposite relative to that of the pristine nano-Si anodes. The two impedance responses are shown in **Figure 3d.** The first semicircle at the high-to-medium frequency range corresponds to the impedance of the SEI film, and the second semicircle at the medium-to-low frequency range corresponds to the impedance of the charge transfer occurring at the surface of the electrode. The inclined line at the low frequency range corresponds to Li^+ diffusion in the bulk electrode.[19, 30] These features suggest that the pristine nano-Si anode had very large impedance

during the charge transfer. However, with the graphene nanosheet coating, the impedance of the SEI film and the charge transfer were significantly reduced in the nanocomposite anode. These results indicate that the graphene nanosheets play two important roles. The first role is facilitation of formation of a stable and dense SEI film by the graphene nanosheet coating, resulting in reduced impedance caused by the SEI film. The second is enhancement of the electronic conductivity of the electrode by the graphene nanosheet matrix, resulting in facilitated surface charge transfer.

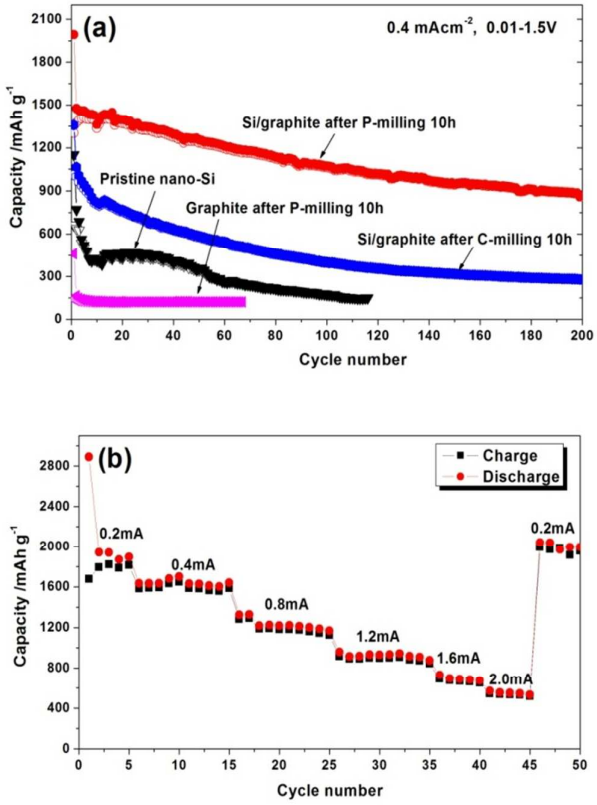

Figure 4. (a) Long-term cycle performance of the P-milled Si/graphene nanocomposite, C-milled Si/graphite composite, and pristine nano-Si and P-milled graphite anodes at 0.4mAcm^{-2}; (b) rate performance of the P-milled Si/graphene nanocomposite in a half cell.

Figure 4 shows the long-term cycling stability, high-rate capability in the half cell of the Si/graphene nanocomposite electrode. As can be seen in **Figure 4a**, the P-milled Si/graphene nanocomposite anode had good cycle performance even after repeatedly charge and discharge for up to 200 cycles at 0.4 mAcm^{-2}. This result shows that it had a stable capacity much higher than that of P-milled pure graphite and pristine nano-Si anodes. Because of the irreversible capacity in the first cycle due to the decomposition of electrolyte and SEI formation, the discharge capacity in

the second cycle is used for the calculation of capacity retention. The specific discharge capacities based on the entire composite weight (Si and graphite) were 1474, 1071, and 866 $mAhg^{-1}$ at the 2nd, 100th, and 200th cycle, respectively. These are equivalent to specific capacities of 2948, 2142, and 1732$mAhg^{-1}$at the 2nd, 100th, and 200th cycle, respectively, based on 50 wt% Si loading and 150 mAh g^{-1}capacity of the P-milled graphite. However, it needs to be pointed out that the P-milled graphite anode had much lower reversible capacity than the theoretical capacity of graphite (372mAh g^{-1}),which should be due to that the now used graphite had relative low activity for Li storage at the applied current and potential. Nevertheless, the discharge capacity loss over 200 cycles was only ~0.21% per cycle, with capacity retention of 58.8% and coulombic efficiency above 99.0% (**Figure S4, Supporting Information**) after 200 cycles, which was much better than those of the previously reported Si–C nanocomposite anodes prepared through other methods.[38–41] As indicated in Figure 4a, the P-milled nanocomposite also showed much higher capacity and cycleability than did the nano-Si/graphite composite prepared by C-milling without assistance of discharge plasma. This difference could be attributed to the preferred formation of graphene nanosheets over amorphous carbon due to the use of plasma,[31] and the highly uniform distribution of nano-Si particles inside graphene due to P-milling. Since the nano-Si particles had been tightly coated and connected by the highly conductive graphene nanosheets, the P-milled Si/graphene nanocomposite displayed good rate performance. As shown in **Figure 4b**, a reversible capacity of 1895 mAh g^{-1} was obtained at the end of five charge/discharge cycles at 0.2$mAcm^{-2}$. The capacity at 0.4$mAcm^{-2}$ was 1640 mAh g^{-1}, and decreased to 534 mAh g^{-1} at the increased rate of 2 $mAcm^{-2}$. Surprisingly, the high capacity (1995 mAh g^{-1}) was restored when the current density was reduced again to 0.2$mAcm^{-2}$after cycling at 2$mAcm^{-2}$. A superior long-term cycleability with higher reversible capacity of 1195 $mAhg^{-1}$ after 200 cycles at 0.2 $mAcm^{-2}$ was also observed (**Figure S5**, **Supporting Information**). This excellent recovery of capacity further verifies the superior high-rate capability of the P-milled nanocomposite with graphene nanosheets due to conductive connections and buffering of volumetric change of the active nano-Si particles. Moreover, the thermal shock from the discharge plasma on the Si particles increased the defects on surface and thereby enhanced the lithiation activities and Li^+ diffusion in the electrode.

Nevertheless, this P-milled Si/graphene nanocomposite has a large irreversible capacity of 690 mAh g^{-1} and thus a relative low initial coulumbic efficiency of 65.4% (Figure 3b).These could be

ascribed to the electrolyte decomposition and SEI formation on graphene nanosheet surfaces during the high potential zone, and especially many Li ions were trapped in the loss contact Li_xSi parts at the first discharge during the low potential zone, which cannot be extracted again during charge at the applied current(0.4mAcm^{-2}) and potential(1.5V vs. Li/Li$^+$).

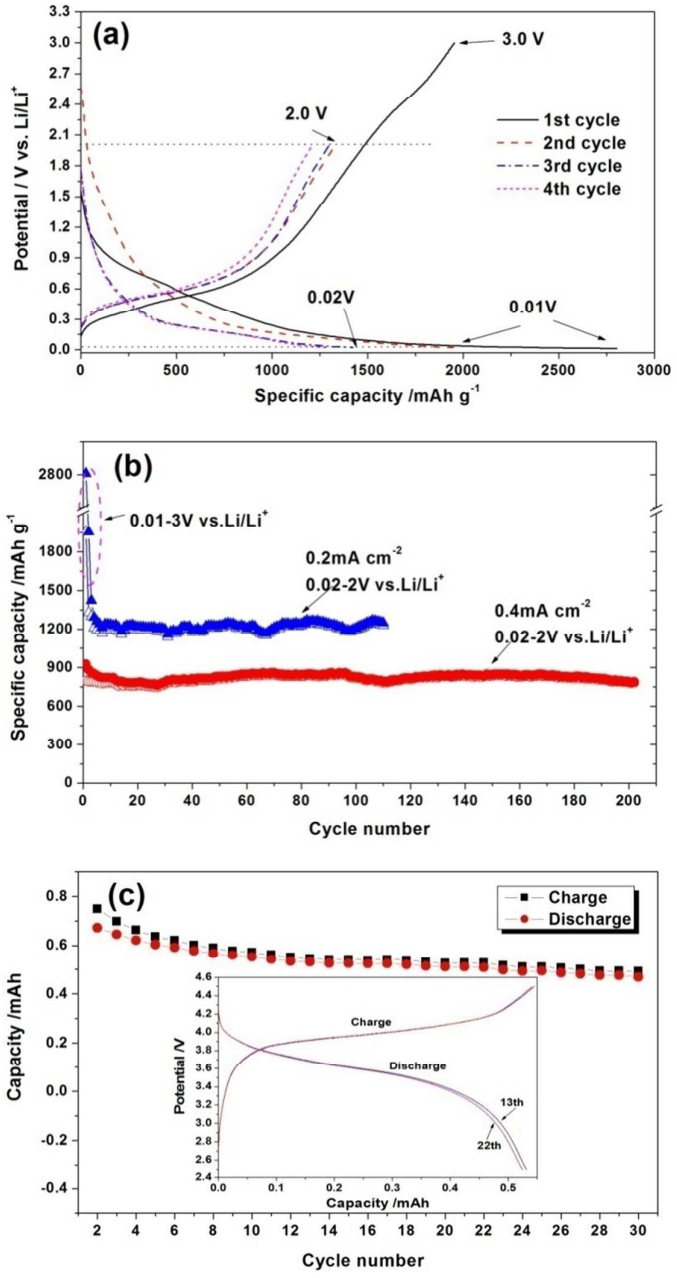

Figure5 (a) Initial four discharge–charge profiles at 0.2mAcm^{-2} of the P-milled Si/graphene nanocomposite among 0.01-3V, and then 0.02-2V vs. Li/Li$^+$; (b) lone-term cycle performance of the P-milled Si/graphene nanocomposite between 0.02 and 2V vs. Li/Li$^+$ at current densities of 0.2, and 0.4mAcm^{-2}, respectively; (c) capacity and charge–discharge profiles (inset) versus cycle number between 2.5 and 4.5V for a coin-type full cell with Si/graphene nanocomposite anode and $LiMn_2O_4$ cathode.

As can be seen in **Figure 5a**, a charge (lithium extraction) capacity of 660mAh g^{-1} can be released between 1.5 and 3.0V at lower current density of 0.05mAcm^{-2}, resulting in a higher initial coulombic efficiency of 70% with discharge current density of 0.2mAcm^{-2}. And further it has been reported by Cui et al. that the initial coulombic efficiency of Si based nanocomposite could be much increased by a facile and rapid prelithiation method.[10] In addition, the long plateaus near the end of discharge (0.02-0.01V) should be attributed to two-phase regions involving that amorphous Li-Si phase undergoes an abrupt crystallization to a $Li_{15}Si_4$ Phase, [42] which has been associated with high internal stresses, leading to particle cracking and capacity fading. These suggest that better cycling should result if these Si/graphene nanocomposite anodes were restricted to cycle above 0.02V.

As shown in **Figure 5b**, it is apparent that there was superior cycling of the cells which were restricted to cycle between 0.02 and 2V after one cycle among 0.01-3V. At a constant current density of 0.2 mAcm^{-2}, a reversible capacity of about 1200mAh g^{-1} keeps stable among 110 cycles. And while the current density increases to 0.4 mAcm^{-2}, the anode delivered a reversible capacity of 789mAh g^{-1} and coulombic efficiency above 99.2% after 200cycle, indicating that the discharge capacity loss over 200 cycles was only ~0.07% per cycle. This is three time lower than that cycling between 0.01 and 1.5V as shown in Figure 4a, and also further confirming the combination of high capacity and good cycleability of these P-milling nanocomposite anodes.

To investigate further the practicality of the Si/graphene nanocomposite, we assembled a coin-type full cell in which the nanocomposite anode was coupled to a $LiMn_2O_4$ cathode. **Figure 5c** illustrates the response of this cell in terms of capacity (mAh) versus cycle number between 4.5 and 2.5V. The cycling tests showed that the practical working voltage of the full cell ranged between 3.2 and 4.2 V, with average discharge and charge voltages 3.6 and 4.0V, respectively, indicating that the Si/graphene nanocomposite anode maintained high working voltage comparable to that of a graphite anode. Furthermore, the full cell could cycle with stable capacities, and the charge–discharge efficiencies were above 97%. These results confirm the practical relevance of the P-milled Si/graphene nanocomposite as an anode material in LIBs. Additionally, the electrochemical performance of the Si/graphene based nanocomposite could be further optimized by tuning the material composition, nanostructure, and P-milling process as below.

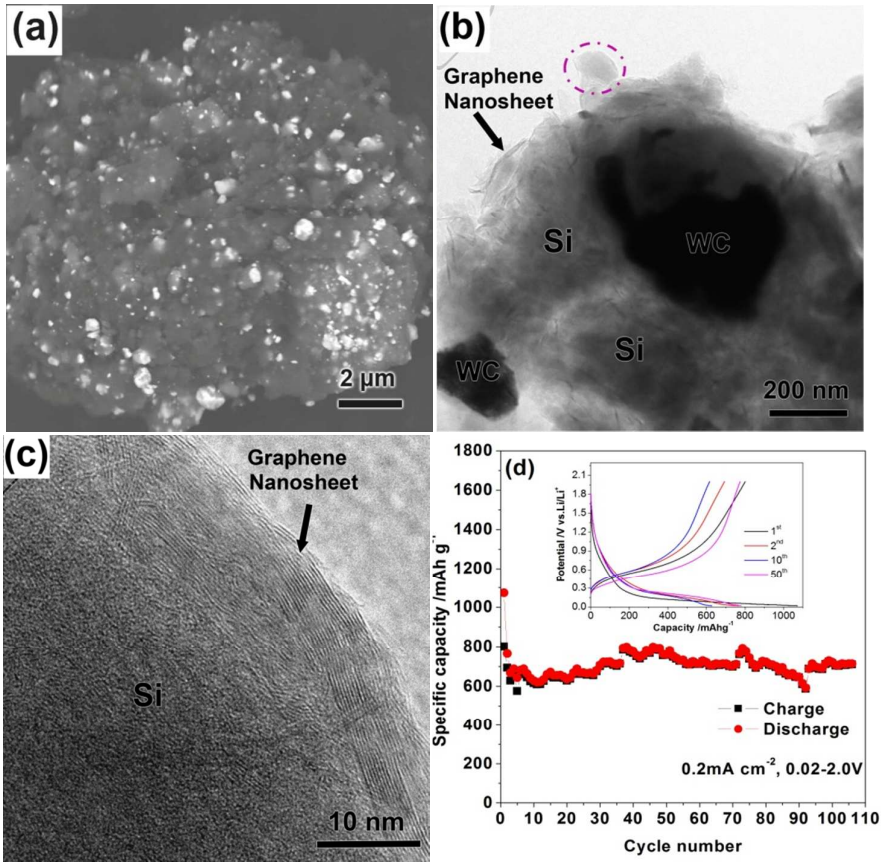

Figure 6 (a) SEM image, (b) TEM image of the microsized spherical granules of the Si-WC/graphene nanocomposite formed after P-milling of Si-WC mixture and graphite for 10h; (c) HRTEM image for the area marked with dotted circle in (b), revealing the graphene nanosheet nature coated outside the Si particle; (d) cycle performance and charge-discharge profiles (insert) of the Si-WC/graphene nanocomposite at 0.2mAcm^{-2} between 0.02 and 2 V.

In order to meet the practicality and reduce the costs, micro-sized Si (1~3μm, Figure S1), instead of the nano-Si, mixed with micro-sized WC and graphite, was also treated by P-milling combined with C-milling to form a Si-WC/graphene nanocomposite. The adding of WC is in purpose of refining Si in milling. XRD results (**Figure S6, Supporting Information**) revealed the dramatically refinement of the Si and graphite after P-milling. **Figure 6a** shows the SEM image of the microsized spherical granules of the nanocomposite. It is obvious that the Si had been refined to nanoscale, whereas the WC particles (bright spots) were homogeneously dispersed inside the matrix. TEM image in **Figure 6b** clearly indicate the "core-shell-shell" structure of this nanocomposite, in which the WC particles were surrounded by nanosized Si to form a spherical granule, with graphene nanosheets uniformly coated outside. The graphene nanosheet nature could be further confirmed by the HRTEM image in **Figure 6c**, which reveals that a Si particle was tightly coated by graphene

nanosheets of less than 10 nm thicknesses, being similar to those of the composite directly using nano-Si shown in Figure 2c and d. These suggest that graphene nanosheets were easy to peel from graphite and tend to coat outside the Si particles after treating by P-milling, which was independent on the morphology of the Si raw materials. In this "core-shell-shell" structure of Si-WC/graphene nanocomposite, the submicro-sized WC cores could act as the cornerstones for the nanosized Si and withstand their pulverizations and aggregations, while the outside shell of graphene nanosheets could much enhanced the electronic conductivity among Si-WC granules, as well as between the Si and current collectors. These lead to a superior cycleability for the Si-WC/graphene nanocomposite.

As could be seen in **Figure 6d**, cycling between 0.02 and 2 V at current density of 0.2mAcm^{-2}, the Si-WC/graphene nanocomposite anode delivers a discharge capacity of 1072mAhg^{-1} and a charge capacity of 801mAhg^{-1} at the first cycle, respectively, implying an initial coulombic efficiency of 74.7%. After a fast decay among the first five cycles, the reversible capacities gradually increase from 644mAh g^{-1} at the 5th cycle to 730mAhg^{-1} at the 100th cycle. The wavy variation of the capacities should be induced by the temperature changes of winter (10~25℃) in our labs without thermostatic environment. Nevertheless, the charge-discharge curves inserted in **Figure 6d** reveal the overlapping lithiation plateaus around 0.2V and delithiation plateaus at 0.5V, which are similar to those of the Si/graphene anodes shown in Figure 3b and Figure 5a. These suggest that in-situ formed nanosized Si was the dominant reactance in the Si-WC/graphene nanocomposite electrode, which contributed high capacities and superior cycleability. It should be attributed to that the nanosized Si particles were supported by the conductive rigid WC skeletons and meanwhile completely coated by the high conductive graphene nanosheets, leading to high structure stability of electrode to alleviate its volume expansion during charge/discharge. This further confirmed the validities of the plasma-assisted milling for mass production of high performance Si/graphene based anode materials for LIBs.

4. Conclusion

A Si/graphene nanocomposite was prepared as an anode for LIBs by using a one-step method of P-milling for the first time. The nanocomposites consisted of microsized spherical granules possessing a unique structure of nano-Si particles each tightly coated and connected by 20 graphene nanosheets less than 10nm thick. This Si/graphene nanocomposite demonstrated high capacity,

good cycleability, and excellent high-rate capability. Its discharge capacity loss over 200 cycles was only ~0.21% per cycle, with capacity retention of 866 $mAhg^{-1}$ and coulombic efficiency >99.0% after 200 cycles at 0.4$mAcm^{-2}$ between 0.01 and 1.5V,while a much lower decay rate of 0.07% was realized between 0.02 and 2.0V. Si-WC/graphene nanocomposite, with better cycleability, was also prepared to further confirm the validities of the P-milling for mass production of high performance anode materials for LIBs. These superior electrochemical properties of the nanocomposites are mainly attributed to the unique milling processes and the formed structure. That is, the discharge plasma and the nano-Si acted as nanomillers to help to form many graphene nanosheets in the composite, which protected well the nano-Si particles and highly enhanced the structure stability and conductivity of the electrodes. The Si/graphene based nanocomposites prepared by P-milling were much more cost-effective and easy to scale up and therefore had good potential for use in large-scale applications.

Acknowledgments

This work was supported by the National Science Foundation of China under Project Nos.51201065 and 51231003, by the Guangdong National Science Foundation under Project S2012040008050, the Doctorate Foundation of Ministry of Education under Projects 20120172120007and 2014ZZ0002.

References

[1] M. Winter, J. O. Besenhard, M. E. Spahr, P. Novak, *Adv. Mater.* **1998**,*10*,725
[2] J. L. Tirado, *Mater. Sci. Eng. R,* **2003**, *40*, 103.
[3] D. Larcher, S. Beattie, M. Morcrette, K. Edstrom, J.C. Jumas, J.M. Tarascon, *J. Mater. Chem.* **2007**, *17*, 3759.
[4] R.Z.Hu, M. Zhu, H. Wang, J.W. Liu, L. Z. Ouyang, J.Zou, *Acta Mater.* **2012**, *60*, 4695**.**
[5] H. Li, X. J. Huang, L. Q. Chen, Z. G. Wu, Y. Liang, *Electrochem. Solid-State Letters,* **1999**, *2*, 547
[6] B. Gao, S.Sinha, L. Fleming, O. Zhou, *Adv. Mater.* **2001**, *13*, 816
[7] W. Wang, M. K. Datta, P. N. Kumta, *J. Mater. Chem*. **2007**, *17*, 3229
[8]H. Ma, F. Y. Cheng, J. Chen, J. Z. Zhao, C. S. Li, Z. L. Tao, J. Liang, *Adv. Mater*. **2007**,*19*, 4067
[9]C. K. Chan, H. Peng, G. Lin, K. McIlwrath, X. F. Zhang, R. A. Huggins, Y. Cui, *Nat. Nanotechnol.* **2008**, *3*, 31–35
[10] Q.Zhang, W.Zhang, W. Wan, Y. Cui, E. Wang, *Nano Lett*. **2010**, *10*, 3243
[11] H. Kim, B. Han, J. Choo, J. Cho, *Angew. Chem., Int. Ed.*, **2008**, *47*, 10151
[12] X. Xin, X. F. Zhou, F. Wang, X. Y. Yao, X. X. Xu, Y.M. Zhu, Z. P Liu, *J. Mater. Chem.*, **2012**, *22*, 7724

[13] T. D. Hatchard, M. N. Obrovac, J. R. Dahn, *J. Electrochem. Soc.* **2006**, *153*, A282
[14] G.X. Wang, L. Sun, D.H. Bradhurst, S. Zhong, S.X. Dou, H.K. Liu, *J. Alloys Compd.* **2000**, *306*, 249.
[15] I. Seok Kim , G. E. Blomgren, P. N. Kumta, *Electrochem. Solid-State Lett.* **2003**,*6*, A157
[16] M. S. Park , S. Rajendran, Y. M. Kang, K. S. Han, Y. S. Han, J.Y. Lee, *J. Power Sources*, **2006**, *158*, 650
[17] N. Dimov, S. Kugino, M. Yoshio, *J. Power Sources*, **2004**, *136*, 108
[18]B. Fuchsbichler, C. Stangl, H. Kren, F. Uhlig, S. Koller, *J. Power Sources*, **2011**, *196*, 2889
[19]Y.S. Hu, R. D. Cakan, M. M. Titirici, J. O. Muller, R. Schlogl, M. Antonietti, J. Maier, *Angew. Chem., Int. Ed.* **2008**, *47*,1645.
[20] Y. J. Kwon, J. Cho, *Chem. Commun.* **2008**, *9*, 1109.
[21]S. Xin, Y.G. Guo, L.J.Wan. *Acc. Chem. Res.* **2012**, *45*, 1759.
[22] Y. S. He, P. Gao, J. Chen, X. Yang, X. Liao, J. Yang, Z.F. Ma, *RSC Adv.*, **2011**, *1*, 958
[23] (a) X. Zhou, Y. Yin, L. J. Wan, Y. G. Guo, *Adv. Energy Mater.* **2012**, *2*, 1086; (b)X. Zhou, Y. Yin, L. J. Wan, Y. G. Guo, *Chem. Commun.* **2012**, *48*, 2198.
[24](a)X. Zhou, A. Cao, L.J. Wan, Y. G. Guo, *Nano Res.***2012**, *5*, 845; (b)X. Zhou, L. J. Wan, Y. G. Guo, *Small*, **2013**, *9*, 2684
[25] A. Magasinski, P. Dixon, B. Hertzberg, A. Kvit, J. Ayala, G.Yushin, *Nat. Mater.* **2010**, *9*, 353
[26] M. Holzapfel, H. Buqa, W. Scheifele, P. Novaka, F. M. Petrat, *Chem. Commun.* **2005**,*12*, 1566.
[27] Y. NuLi, B. F. Wang, J. Yang, X. X.Yuan, Z. F. Ma, *J.Power Sources*, **2006**,*153*, 371
[28] T. Li, Y.L. Cao, X.P. Ai, H.X. Yang, *J. Power Sources*, **2008**, *184*, 473
[29]Z.W. Lu, L.Q. Zhang, X. J. Liu, *J. Power Sources*, **2010**, *195*,4304
[30] X. L. Chen, X. L. Li, F. Ding, W. Xu, J. Xiao, Y. L. Cao, P. Meduri, J. Liu, G. L. Graff, J. G. Zhang, *Nano Lett.* **2012**, *12*, 4124.
[31] L. Hui, R.Z.Hu, M.Q.Zeng, J.W.Liu, M.Zhu, *J. Mater. Chem*. **2012**, *22*, 8022
[32] H. Liu, R. Z. Hu, W. Sun, M.Q. Zeng, J.W. Liu, L.C. Yang, M. Zhu, *J. Power Sources*, **2013**, *242*, 4304
[33] L.Y. Dai, B. Cao, M. Zhu, *Acta Metall. Sin.***2006**, *19*, 411
[34] M. Zhu, L.Y. Dai, N.S. Gu, B. Cao, L.Z. Ouyang, *J. Alloys Compd.* **2009**, *478*,624.
[35] B.C. Yu, Y. Hwa, J. H. Kim, H.J. Sohn, *J.Power Sources,* **2014**, doi: 10.1016/ j.jpowsour. 2014.02.109.
[36]C. Suryanarayana, *Prog. Mater. Sci.* **2001**, *46*, 1.
[37] I.Y. Jeon, H. J. Choi, S. M. Jung, J. M. Seo, M. J. Kim, L.M. Dai, J. B. Baek, *J. Am. Chem. Soc.* **2013**, *135*, 1386
[38]S. Cahen, R. Janot, L. Laffont-Dantras, J. M. Tarascon, *J. Electrochem. Soc.* **2008**, *155*, A512
[39] L.W. Ji, H. H. Zheng, A. Ismach, Z.K. Tan, S D.Xun, E. Lin, V. Battaglia, V. Srinivasan, Y.G. Zhang, *Nano Energy*, **2012**,*1*,164
[40] S. H. Woo, J. H. Park, S. W. Hwang, D. Whang, *J. Electrochem. Soc.* **2012**, *159* , A1273.
[41] J. K. Lee, K. B. Smith, C. M. Hayner, H. H. Kung, *Chem. Commun.* **2010**, *46*, 2025.
[42] M. N. Obrovac, L. J. Krause, *J. Electrochem. Soc.* **2007**, *154*, A103